

# Biased Reionisation and Non-Gaussianity in Redshifted 21cm Intensity Maps of the Reionisation Epoch

J. Stuart B. Wyithe<sup>1</sup> and Miguel F. Morales<sup>2</sup>

<sup>1</sup> School of Physics, University of Melbourne, Parkville, Victoria, Australia

<sup>2</sup> MIT Kavli Institute, 77 Massachusetts Ave., Cambridge, MA 02139

Email: [swyithe@physics.unimelb.edu.au](mailto:swyithe@physics.unimelb.edu.au) , [mmorales@space.mit.edu](mailto:mmorales@space.mit.edu)

25 September 2018

## ABSTRACT

Spatial dependence in the statistics of redshifted 21cm fluctuations promises to provide the most powerful probe of the reionisation epoch. In this paper we consider the second and third moments of the redshifted 21cm intensity distribution using a simple model that accounts for galaxy bias during the reionisation process. We demonstrate that skewness in redshifted 21cm maps should be substantial throughout the reionisation epoch and on all angular scales, owing to the effects of galaxy bias which leads to early reionisation in over-dense regions of the IGM. The variance (or power-spectrum) of 21cm fluctuations will exhibit a minimum in redshift part way through the reionisation process, when the global ionisation fraction is around 50%. This minimum is generic, and is due to the transition from 21cm intensity being dominated by over-dense too under-dense regions as reionisation progresses. We show that the details of the reionisation history, including the presence of radiative feedback are encoded in the evolution of the auto-correlation and skewness functions with redshift and mean IGM neutral fraction. The amplitudes of fluctuations are particularly sensitive to the masses of ionising sources, and vary by an order of magnitude for astrophysically plausible models. We discuss the detection of skewness by first generation instruments, and conclude that the Mileura Widefield Array–Low Frequency Demonstrator will have sufficient sensitivity to detect skewness on a range of angular scales at redshifts near the end of reionisation, while a subsequent instrument of 10 times the collecting area could map out the evolution of skewness in detail. The observation of a minimum in variance during the reionisation history, and the detection of skewness would both provide important confirmation of the cosmological origin of redshifted 21cm intensity fluctuations.

**Key words:** cosmology: diffuse radiation, large scale structure, theory – galaxies: high redshift, inter-galactic medium

## 1 INTRODUCTION

The primordial density field as revealed in maps of the Cosmic Microwave Background may be described as a Gaussian random field. In other words, the distribution of over-densities in the Fourier decomposition of the field is Gaussian at all spatial frequencies, so that the statistics of the field may be described by a single number (the variance) as a function of spatial scale. This scale dependent variance is referred to as the power-spectrum. On large enough scales we might also expect the statistics for 21cm emission to be Gaussian, since over-dense regions have more hydrogen, and therefore a larger 21cm intensity. On small scales this Gaussianity will be broken by the presence of HII regions. Thus

much attention has focused on the prospects of measuring the power-spectrum of 21cm emission, as well as the use of the power-spectrum to probe the astrophysics of reionisation (e.g. Zaldarriaga et al. 2004; Morales & Hewitt 2004; Furlanetto et al. 2004).

In regions that are over-dense, galaxies will be over-abundant for two reasons: first because there is more material per unit volume to make galaxies, and second because small-scale fluctuations need to be of lower amplitude to form a galaxy when embedded in a larger-scale over-density (the so-called *galaxy bias*; see Mo & White 1996). Regarding reionisation of the intergalactic medium (IGM), the first effect will result in a larger density of ionising sources. However this larger density will be compensated by the increased

density of gas to be ionised. Furthermore, the increase in the recombination rate in over-dense regions will be counteracted by the galaxy bias in over-dense regions. The process of reionisation also contains several layers of feedback. Radiative feedback heats the IGM and results in the suppression of low-mass galaxy formation (Efstathiou, 1992; Thoul & Weinberg 1996; Quinn et al. 1996; Dijkstra et al. 2004). This delays the completion of reionisation by lowering the local star formation rate, but the effect is counteracted in over-dense regions by the biased formation of massive galaxies. The radiation feedback may therefore be more important in low-density regions where small galaxies contribute more significantly to the ionising flux.

Wyithe & Loeb (2007) have modeled the density dependent reionisation process using a semi-analytic model that incorporates the features described above, and so captures the important physical processes. This model demonstrates that galaxy bias leads to enhanced reionisation in over-dense regions. Because this bias operates on the exponential tail of the Press-Schechter (1974) mass function, the enhancement of ionisation is not linear with over-density. As a result, galaxy bias leads to a non-Gaussian distribution of 21cm brightness temperature in intensity maps of reionisation. This effect was discussed by Lidz et al. (2006) using detailed numerical simulations. Lidz et al. (2006) found that the contribution of a third order term in the power-spectrum will be comparable to the second order term at an epoch where the IGM is approximately 50% ionised. While comparison with data may require detailed numerical simulations of the sort described in Lidz et al. (2006), computationally cheap semi-analytic models are useful for exploring which physical parameters will be probed by the detection of angular fluctuations in the 21cm intensity. In this paper we explore the dependence of observables on the values of parameters of interest like the clumping of the IGM and the minimum mass for galaxy formation. We also discuss the prospects for detection of the third moment (skewness) with first and second generation low-frequency arrays.

In § 2 and § 3 we describe our model for density dependent reionisation, and the resulting redshifted 21cm intensity probability distribution (including calculation of its second and third moments). We describe the features of the auto-correlations and skewness functions that correspond to different physical parameters that are important for the reionisation epoch. We then discuss the measurement of these moments using first and second generation low-frequency arrays (in particular the Mileura Widefield Array–Low Frequency Demonstrator) in § 4 before concluding in § 5. Throughout the paper we adopt the set of cosmological parameters determined by *WMAP* (Spergel et al. 2006) for a flat  $\Lambda$ CDM universe.

## 2 DENSITY DEPENDENT MODEL OF REIONISATION

In this paper we compute the relation between the local over-density and the brightness temperature of redshifted 21cm emission using the model described in Wyithe & Loeb (2007). Here we summarise the main features of the model and refer the reader to that paper for more details.

The evolution of the ionisation fraction by mass  $Q_{\delta,R}$

of a particular region of scale  $R$  with over-density  $\delta$  (at observed redshift  $z_{\text{obs}}$ ) may be written as

$$\begin{aligned} \frac{dQ_{\delta,R}}{dt} = & \frac{N_{\text{ion}}}{0.76} \left[ Q_{\delta,R} \frac{dF_{\text{col}}(\delta, R, z, M_{\text{ion}})}{dt} \right. \\ & \left. + (1 - Q_{\delta,R}) \frac{dF_{\text{col}}(\delta, R, z, M_{\text{min}})}{dt} \right] \\ & - \alpha_B C n_{\text{H}}^0 \left( 1 + \delta \frac{D(z)}{D(z_{\text{obs}})} \right) (1+z)^3 Q_{\delta,R}, \end{aligned} \quad (1)$$

where  $N_{\text{ion}}$  is the number of photons entering the IGM per baryon in galaxies,  $\alpha_B$  is the case-B recombination coefficient,  $C$  is the clumping factor (which we assume, for simplicity, to be constant), and  $D(z)$  is the growth factor between redshift  $z$  and the present time. The production rate of ionising photons in neutral regions is assumed to be proportional to the collapsed fraction  $F_{\text{col}}$  of mass in halos above the minimum thresholds in neutral ( $M_{\text{min}}$ ), and in ionised ( $M_{\text{ion}}$ ) regions. For our fiducial model, we assume  $M_{\text{min}}$  to correspond to a virial temperature of  $10^4$  K, representing the hydrogen cooling threshold, and  $M_{\text{ion}}$  to correspond to a virial temperature of  $10^5$  K, representing the mass below which infall is suppressed from an ionised IGM (Dijkstra et al. 2004). In a region of co-moving radius  $R$  and mean over-density  $\delta(z) = \delta D(z)/D(z_{\text{obs}})$  [specified at redshift  $z$  instead of the usual  $z = 0$ ], the relevant collapsed fraction is obtained from the extended Press-Schechter (1974) model (Bond et al. 1991) as

$$F_{\text{col}}(\delta, R, z) = \text{erfc} \left( \frac{\delta_c - \delta(z)}{\sqrt{2} ([\sigma_{\text{gal}}]^2 - [\sigma(R)]^2)} \right), \quad (2)$$

where  $\text{erfc}(x)$  is the error function,  $\sigma(R)$  is the variance of the density field smoothed on a scale  $R$ , and  $\sigma_{\text{gal}}$  is the variance of the density field smoothed on a scale  $R_{\text{gal}}$ , corresponding to a mass scale of  $M_{\text{min}}$  or  $M_{\text{ion}}$  (both evaluated at redshift  $z$  rather than at  $z = 0$ ). In this expression, the critical linear over-density for the collapse of a spherical top-hat density perturbation is  $\delta_c \approx 1.69$ .

The model assumes that on large (linear-regime) scales most ionising photons are absorbed locally, so that the ionisation of a region is caused by nearby ionisation sources. This assumption is certainly justified during the early stages of reionisation, when the mean free path for ionising photons is short. However even later in the reionisation process, the mean free-path always remains smaller than the characteristic HII bubble size (it could be smaller if mini-halos or pockets of residual HI block ionising photons between the sources and the edge of the HII region.) Our local ionisation assumption is therefore valid as long as the characteristic bubble size is smaller than the spatial scale of the correlations we consider. In this paper we consider scales of 1-25 arc-minutes which will be of interest to upcoming 21cm experiments, corresponding to co-moving scales of 2-50 Mpc. These scales are larger than the mean-free-path of ionising photons near the end of reionisation (Fan et al. 2006).

As an example, we find the value of  $N_{\text{ion}}$  that yields overlap of ionised regions at the mean density IGM by  $z \sim 6$  (White et al. 2003). Equation (1) may be integrated as a function of  $\delta$ . At a specified redshift, this yields the filling fraction of ionised regions within the IGM on various scales  $R$  as a function of over-density. We may then calculate the

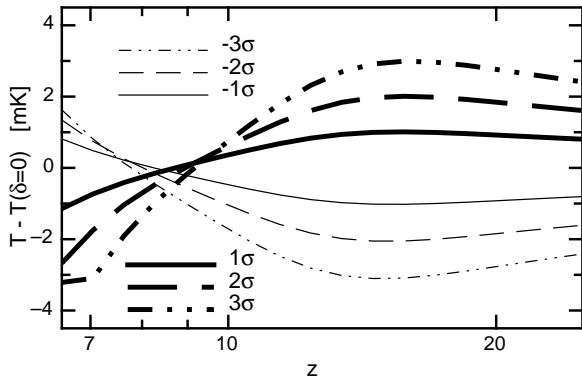


**Figure 1.** The difference in brightness temperature between over or under-dense regions, and the IGM at mean density as a function of redshift. The lines represent regions at redshift  $z$  that are  $-3\sigma$ ,  $-2\sigma$ ,  $-1\sigma$ ,  $0\sigma$ ,  $1\sigma$ ,  $2\sigma$  or  $3\sigma$  fluctuations in the smoothed density field. We assumed a clumping factor of  $C = 10$  and an angular scale of  $10'$ .

corresponding 21cm brightness temperature contrast

$$T(\delta, R) = 22\text{mK}(1 - Q_{\delta, R}) \left(1 + \frac{4}{3}\delta\right), \quad (3)$$

where the pre-factor of  $4/3$  on the over-density refers to the spherically averaged enhancement of the brightness temperature due to peculiar velocities in over-dense regions (Bharadwaj & Ali 2005; Barkana & Loeb 2005).

The predicted evolution of the brightness temperature of regions of IGM at fixed angular scale is plotted in Figure 1. For clarity we have plotted  $T - T(\delta = 0)$ , i.e. the difference in brightness temperature between the over or under-dense region, and the IGM at mean density. Each line in the figure represents a region that is a  $-3\sigma$ ,  $-2\sigma$ ,  $-1\sigma$ ,  $0\sigma$ ,  $1\sigma$ ,  $2\sigma$  or  $3\sigma$  fluctuation in the smoothed density field at redshift  $z$ . Here we assumed a clumping factor of  $C = 10$  and an angular scale of  $10'$ , where  $\theta = R/d_A(z)$  and  $d_A$  is the angular diameter distance. At high redshift the curves are symmetric about zero, as expected for linear fluctuations in the primordial density field. As reionisation proceeds the brightness temperature (relative to the mean IGM) is initially quite insensitive to redshift. However at later times the brightness temperature of over-dense regions decreases, while the brightness temperature of under-dense regions increases (again when compared to the mean IGM). Finally, reionisation is completed in over-dense regions of the IGM first, as may be seen in the  $3\sigma$  fluctuation which is reionised at  $z \sim 7$ , prior to the mean IGM at  $z = 6$ . Therefore at some point during the reionisation history there must be a transition between bright patches of 21cm emission being observed in over-dense regions, too bright patches being observed in under-dense regions. This transition results in an epoch of nearly uniform brightness temperature (uniform when smoothed on an angular scale larger than the typical HII region) of the IGM. Figure 1 shows that in our models this transition occurs near a redshift of  $z \sim 8 - 9$ . The epoch of near uniform temperature across the IGM has interesting consequences for the variance in smoothed 21cm intensity maps. This topic will be discussed in the following section.

Figure 1 also shows that reionisation skews the bright-

ness temperature towards low values, owing to the dominant effect of galaxy bias. A point of interest here is that once reionisation begins, this results in the brightness temperature of both over- and under-dense regions being lower than the brightness temperature of the IGM at mean density (we note that the mean is not found to depend on angular scale as required for consistency). Since the underlying probability distribution of over-densities  $dP/d\delta$  is known (a Gaussian of variance  $\sigma D$ ), we may compute the observed probability distribution for  $T$ ,

$$\frac{dP}{dT}(\theta) \propto \frac{dP}{d\delta} \left| \frac{\partial \delta}{\partial T} \right|. \quad (4)$$

This distribution corresponds to fluctuations in redshifted 21cm emission on angular scales  $\theta$ . Example distributions are shown in Figures 2 and 3.

Firstly we discuss the evolution of the distribution with redshift at fixed angular scale. In Figure 2, distributions are shown assuming a clumping factor of  $C = 10$  and an angular scale of  $10'$ , at redshifts of  $z = 6.5$ ,  $z = 7$ ,  $z = 8.5$ ,  $z = 10$ ,  $z = 13$  and  $z = 22$ . The large symbols in this figure show the value of  $T - T(\delta = 0)$  corresponding to regions that are  $-2\sigma$ ,  $-1\sigma$ ,  $0\sigma$ ,  $1\sigma$  and  $2\sigma$  fluctuations in the smoothed density field respectively. The lower right hand panel clearly shows the Gaussian distribution at high redshift, with evenly spaced values of  $T$  corresponding to the  $\pm 1\sigma$  and  $\pm 2\sigma$  points. At slightly lower redshift, the lower central panel shows that the Gaussian has become a little wider due to linear growth, with the high  $T$  tail slightly truncated (due to the onset of skewness), as may be seen by comparing the relative likelihoods for temperature corresponding to the positive and negative over-density fluctuations. At a redshift of  $\sim 10$  in this example (lower left panel), one gets a narrower and very skewed distribution. At this point the positive over-densities still correspond to larger than average brightness temperature, but the difference in brightness temperature between regions of mean density and  $+2\sigma$  fluctuations is small. The upper right panel shows the distribution at  $z = 8.5$  (the minimum). At this redshift, the distribution is both very asymmetric and narrow, but in addition, the monotonic dependence of brightness temperature with over-density is broken. Indeed, the mean IGM density corresponds to the largest brightness temperatures, while the brightness temperatures of  $+1\sigma$  and  $-1\sigma$ , and of  $+2\sigma$  and  $-2\sigma$  density fluctuations are almost the same. At lower redshifts (upper-central and upper-left panels) the width and skewness of the distributions both increase, and a monotonic relation between the over-density and brightness temperature is restored, though the order is reversed relative to high redshift.

In Figure 3 distributions are shown assuming a clumping factor of  $C = 10$  and a redshift of  $z = 7$ , at angular scales of  $5'$ ,  $10'$ ,  $15'$  and  $20'$  and  $z = 7$ . The distribution is valid on angular scales sufficiently large that no region on that scale is fully ionised. On small enough scales the distribution must be described using a model that calculates the size distribution of individual HII regions (e.g. Furlanetto et al. 2004). However as may be seen from Figure 3, our model describes the distribution  $dP/dT$  for  $\theta \gtrsim 5'$  at  $z = 7$ , and for all angles of interest to up-coming 21cm experiments at higher redshifts. At large angular scales (lower-right panel) the distribution is narrow and close to Gaussian. By compar-

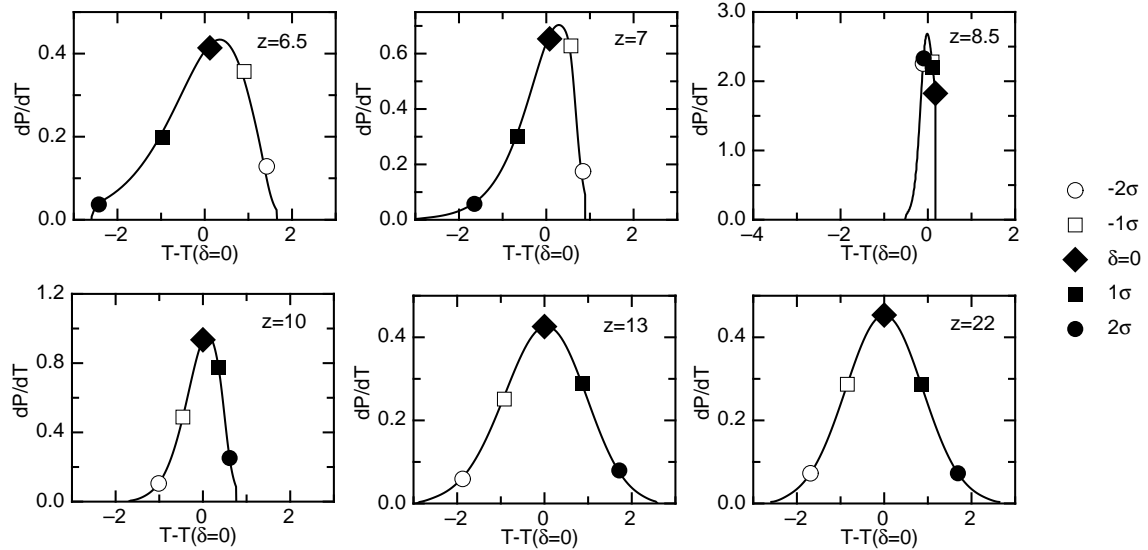


**Figure 2.** The probability distribution of brightness temperature  $dP/dT$ . The horizontal axis shows the difference in brightness temperature between over or under-dense regions, and the IGM at mean density  $[T - T(\delta = 0)]$ . Distributions are shown assuming a clumping factor of  $C = 10$  and an angular scale of  $10'$ , at redshifts of  $z = 6.5$ ,  $z = 7$ ,  $z = 8.5$ ,  $z = 10$ ,  $z = 13$  and  $z = 22$ . The large symbols show the value of  $T - T(\delta = 0)$  corresponding to regions that are  $-2\sigma$  (filled circle),  $-1\sigma$  (filled square),  $0\sigma$  (filled diamond),  $1\sigma$  (empty square) and  $2\sigma$  (empty circle) fluctuations in the density field and correspond to lines in Figure 1.

ing the brightness temperatures corresponding to the  $\pm 1\sigma$  and  $\pm 2\sigma$  regions of IGM with the redshift dependent distributions in Figure 2 we see that even though the distribution is still close to Gaussian it already includes the effects of galaxy bias, since the brighter than average regions are formed by under-dense regions of IGM. As the angular scale is decreased the width of the distributions increases, and the skewness towards small  $T$  increases.

Figures 2 and 3 explicitly demonstrate the introduction of skewness into the distribution of  $T(\theta)$ . The skewness of 21cm intensity maps, and its dependence on model parameters will be discussed in more detail in the following section.

### 3 THE VARIANCE AND SKEWNESS OF 21CM MAPS

In this section we calculate the second and third moments of the probability distributions of  $T$  in redshifted 21cm intensity maps, as functions of angular scale and redshift. Given the structure of our semi-analytic model for reionisation, it is natural to discuss the moments of the real space intensity fluctuations smoothed within top-hat window functions of angular radius  $\theta$ .

The second moment of these distributions corresponds to the auto-correlation function of brightness temperature smoothed on an angular radius  $\theta$ :

$$\langle (T - \langle T \rangle)^2 \rangle = \left[ \frac{1}{\sqrt{2\pi}\sigma(R)} \int d\delta (T(\delta, R) - \langle T \rangle)^2 e^{-\frac{\delta^2}{2\sigma(R)^2}} \right], \quad (5)$$

where

$$\langle T \rangle = \frac{1}{\sqrt{2\pi}\sigma(R)} \int d\delta T(\delta, R) e^{-\frac{\delta^2}{2\sigma(R)^2}}, \quad (6)$$

and  $\sigma(R)$  is the variance of the density field (at redshift  $z$ ) smoothed on a scale  $R$ .

A measure of the departure of the statistics from those of a Gaussian random field is provided by the third moment of the distribution  $dP/dT$ . We refer to the third moment as the skewness function of brightness temperature smoothed with top-hat windows of angular radius  $\theta$ .

$$\langle (T - \langle T \rangle)^3 \rangle = \left[ \frac{1}{\sqrt{2\pi}\sigma(R)} \int d\delta (T(\delta, R) - \langle T \rangle)^3 e^{-\frac{\delta^2}{2\sigma(R)^2}} \right]. \quad (7)$$

Examples of auto-correlation and skewness functions are shown in the left and right hand panels of Figure 4 assuming clumping factors of  $C = 10$ ,  $C = 20$  and  $C = 2$ . The auto-correlation function is plotted as a function of  $\theta$  (at  $z = 6.5$ , upper panel), as a function of mean IGM neutral fraction  $x_{\text{HI}}$  (at  $\theta = 10'$ , central panel), and as a function of redshift (at  $\theta = 10'$ , lower panel). In the left and right hand panels of Figure 5 we show examples of auto-correlation and skewness functions for four commonly discussed scenarios of galaxy formation in a neutral and ionised IGM. The four cases presented in Figure 5 show results for the following combinations of  $(T_{\text{min}}, T_{\text{ion}})$ :  $(10^4 \text{K}, 10^5 \text{K})$  corresponding to our fiducial model with star-formation down to the hydrogen cooling threshold in neutral regions plus radiative feedback;  $(10^4 \text{K}, 10^4 \text{K})$  corresponding to a model with no radiative feedback; and  $(10^5 \text{K}, 10^5 \text{K})$  which could correspond to a model where feedback within the galaxy (e.g. from supernovae Dekel & Woo 2003) limits the star formation efficiency in low mass galaxies; and  $(250 \text{K}, 10^5 \text{K})$  corresponding to a model where molecular hydrogen cooling allows star formation to occur in mini-halos below the hydrogen cooling threshold. The clumping factor was assumed to be  $C = 10$  in each case. In all examples presented in Fig-

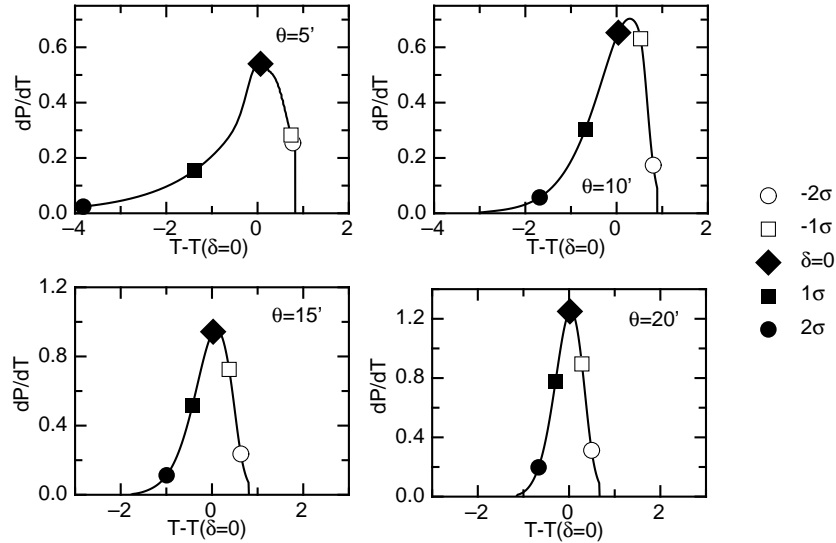


**Figure 3.** The probability distribution of brightness temperature  $dP/dT$ . The horizontal axis shows the difference in brightness temperature between over or under-dense regions, and the IGM at mean density  $[T - T(\delta = 0)]$ . Distributions are shown assuming a clumping factor of  $C = 10$  and a redshift of  $z = 7$ , at angular scales of  $5'$ ,  $10'$ ,  $15'$  and  $20'$ . The large symbols show the value of  $T - T(\delta = 0)$  corresponding to regions that are  $-2\sigma$ ,  $-1\sigma$ ,  $0\sigma$ ,  $1\sigma$  and  $2\sigma$  fluctuations in the density field respectively.

ures 4–5 we have set the efficiency of the ionising sources so as to achieve reionisation in the mean IGM at  $z = 6$ .

We find that the amplitude of the auto-correlation function decreases with angular scale as expected. The amplitude of the skewness also decreases with angular scale. However interestingly, the amplitudes of the auto-correlation and skewness functions do not vary monotonically with redshift or average neutral fraction. In particular, both the variance and skewness of the 21cm intensity field have minima during the reionisation history. At high redshift the skewness goes to zero, since the 21cm map prior to galaxy formation must follow a Gaussian distribution corresponding to the primordial density fluctuations.

This unintuitive behavior was alluded to in Figure 1 and can be understood as follows. Early in the reionisation history, before galaxies have had much influence on the ionisation state of the IGM, the variance is governed by the primordial power-spectrum of fluctuations in the density field, and the skewness is zero. During this early time, the over-dense regions are brighter due to the higher density of neutral IGM there. As galaxies modify the ionisation state of the IGM, the over-dense regions get ionised first, breaking the Gaussianity of the 21cm map. Therefore, once reionisation is underway, the over-dense regions of IGM become fainter in 21cm emission relative to under-dense regions. As was shown in Figure 1, this results in a transition between bright patches of 21cm emission being observed in over-dense regions, too bright patches being observed in under-dense regions. This transition yields an epoch of nearly uniform brightness temperature of the IGM when smoothed at a certain scale, and hence minima in the auto-correlation and skewness functions. At later times, both the variance and the skewness increase as reionisation is completed.

To illustrate this complex behavior in more detail, we plot contours of the auto-correlation and skewness in Figure 6 as functions of redshift and angular scale (upper and

central panels). For comparison we also plot the evolution of the average neutral fraction with redshift (lower panels). Two cases are shown, corresponding to the two models in Figure 5 that include radiative feedback, i.e.  $(T_{\min}, T_{\text{ion}}) = (10^4 \text{K}, 10^5 \text{K})$  [left panels] and  $(T_{\min}, T_{\text{ion}}) = (250 \text{K}, 10^5 \text{K})$  [right panels]. Comparison of the upper and central panels with the lower panels in Figure 6 shows that minima in both the auto-correlation and skewness occur when the ionised fraction is around  $Q \sim 0.5 - 0.7$ , near a redshift of  $z \sim 8 - 9$ . The minimum occurs at higher redshifts for fluctuations measured at smaller angular scales. Comparison of the central and lower panels of Figure 6 show that skewness appears in the 21cm map at the redshift where the reionisation of the IGM begins (at  $z \sim 20$  in this model). However the upper panels show non-zero fluctuations in 21cm emission at earlier times, which are driven by the density fluctuations in the IGM. Note that the two models yield identical fluctuation statistics at  $z \sim 20$ . Finally, Figure 6 shows that the skewness becomes larger in comparison to the auto-correlation amplitude as reionisation proceeds.

In Figures 4 and 5 we demonstrated the dependence of the auto-correlation and skewness functions on model parameters as a function of angle or redshift. Figure 6 demonstrates this dependence more-fully. While the general trends and overall shape are similar in both cases, there are substantial quantitative differences. These plots demonstrate the rich detail on the reionisation history that can be found by considering both the auto-correlation and skewness functions and their evolution. In particular, the amplitudes of the auto-correlation and skewness functions, as well as the epoch and depth of their minima in redshift are sensitive to the details of the reionisation history. The shape of the angular power-spectrum has been shown to encode information on the topology of the reionisation process. Our results show that the evolution of the fluctuation statistics in 21cm intensity maps will provide complementary information on

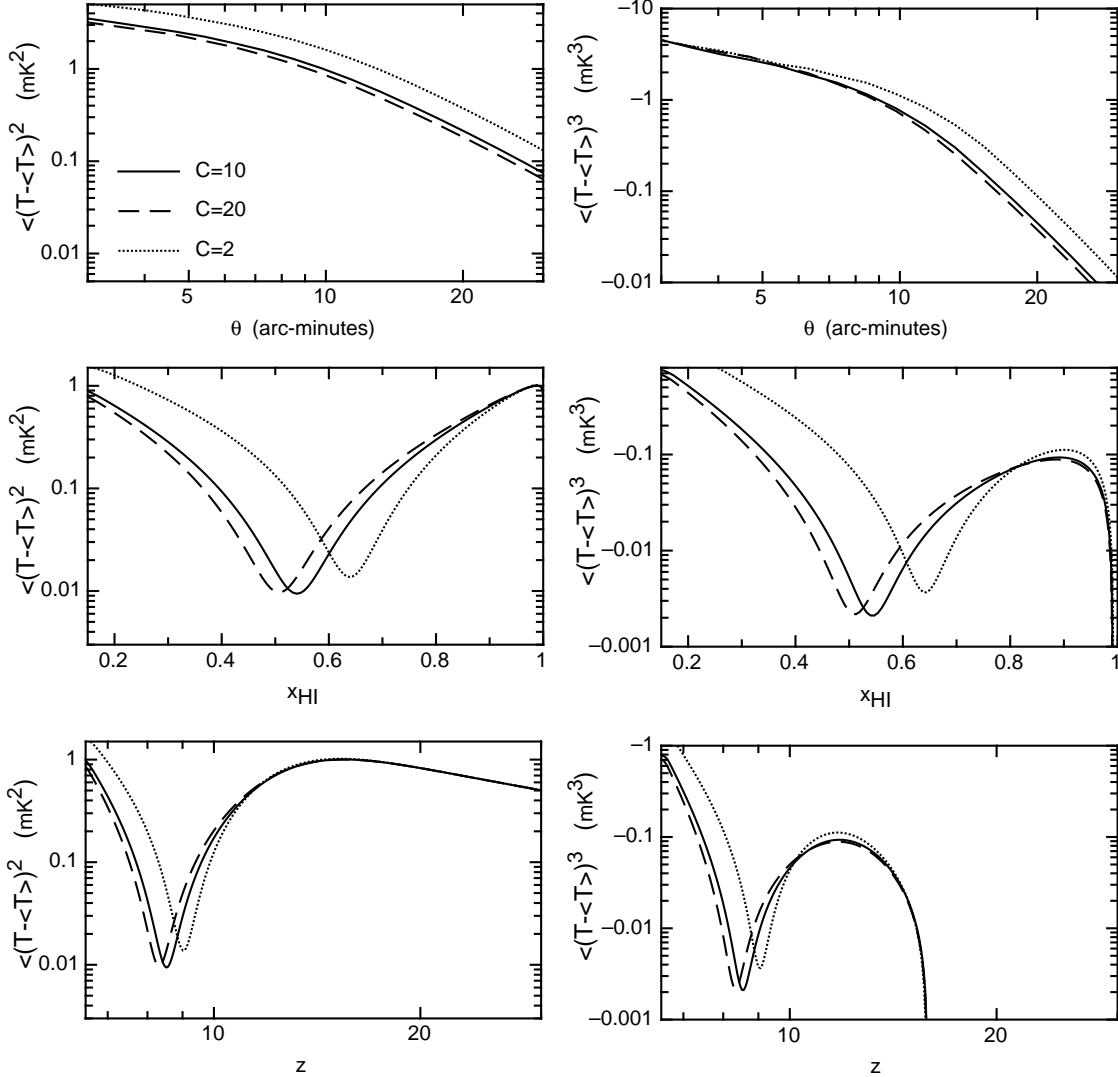


**Figure 4.** *Left:* Examples of auto-correlation functions, assuming clumping factors of  $C = 10$ ,  $C = 20$  and  $C = 2$ . The auto-correlation is plotted as a function of  $\theta$  (at  $z = 6.5$ , *upper panel*), as a function of mean IGM neutral fraction  $x_{\text{HI}}$  (at  $\theta = 10'$ , *central panel*), and as a function of redshift (at  $\theta = 10'$ , *lower panel*). *Right:* Corresponding examples of skewness functions.

the astrophysics of the reionisation epoch. This is the topic of the next section.

### 3.1 Variation of auto-correlation and skewness with model parameters

The free parameters that govern the details of the reionisation history described in equation (1) are the clumping factor  $C$  and the minimum masses for galaxy formation in a neutral ( $M_{\text{min}}$ ) and reionised IGM ( $M_{\text{ion}}$ ). These parameters encapsulate the astrophysics of the IGM, and of the connection between the IGM and ionising sources respectively. In this section we discuss the variation of the auto-correlation and skewness functions with these parameters.

In Figure 4 we demonstrated the variation of the angular auto-correlation and skewness functions with clumping of the IGM. A larger clumping factor results in an increased recombination rate in over-dense regions. At low redshift, where over-dense regions have lower than average 21cm in-

tensity, this increased recombination rate reduces the effect of galaxy bias on the variation of 21cm intensity with over-density by delaying the reionisation of over-dense regions. Thus the observational effect of a large clumping factor in the IGM is to reduce both the variance and the skewness of the distribution of 21cm intensity fluctuations. Conversely at higher redshifts (where over-dense regions have higher than average 21cm intensity), the increased recombination rate results in an increased amplitude for the auto-correlation and skewness functions.

In Figure 5 we demonstrate the dependence of the angular auto-correlation and skewness functions on the minimum mass for galaxy formation in a neutral and ionised IGM. The four cases shown correspond to commonly discussed possibilities for the star formation history at high redshift. Our fiducial model includes radiation feedback by increasing the virial temperature corresponding to the minimum mass from  $T_{\text{min}}$  to  $T_{\text{ion}}$  following reionisation of a region. As a result, once part of a region becomes ionised, the photon produc-

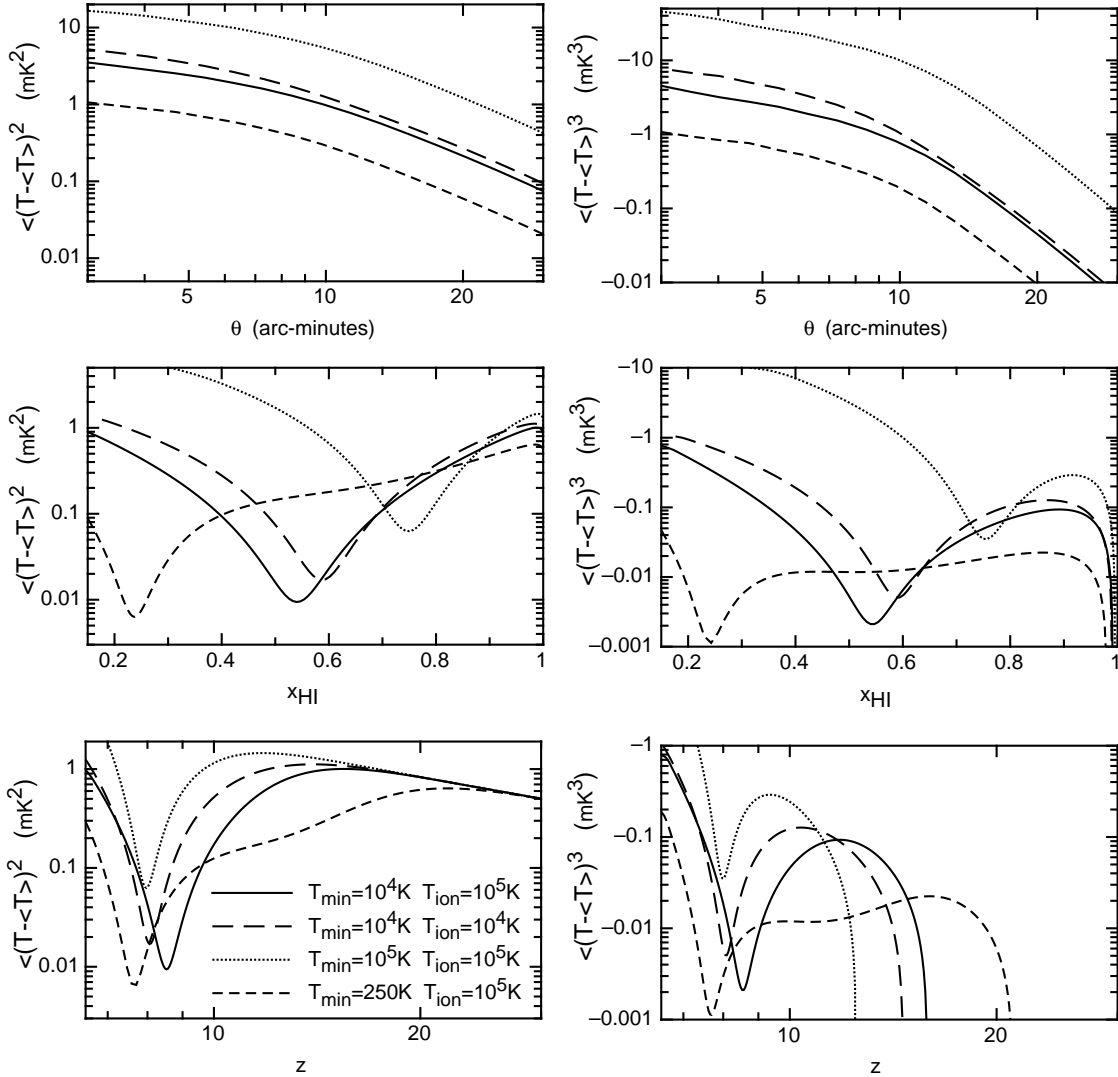


**Figure 5.** *Left:* Examples of auto-correlation functions, assuming sets of  $(T_{\min}, T_{\text{ion}}) = (10^4 \text{K}, 10^5 \text{K})$ ,  $(10^4 \text{K}, 10^4 \text{K})$ ,  $(10^5 \text{K}, 10^5 \text{K})$  and  $(250 \text{K}, 10^5 \text{K})$ . The clumping factor was chosen to be  $C = 10$ . The auto-correlation is plotted as a function of  $\theta$  (at  $z = 6.5$ , *upper panel*), as a function of mean IGM neutral fraction  $x_{\text{HI}}$  (at  $\theta = 10'$ , *central panel*), and as a function of redshift (at  $\theta = 10'$ , *lower panel*). *Right:* Corresponding examples of skewness functions.

tion there is suppressed, slowing down the subsequent ionisation rate relative to more neutral regions. Comparison of the fiducial model having  $(T_{\min}, T_{\text{ion}}) = (10^4 \text{K}, 10^5 \text{K})$  with the case of no feedback  $(T_{\min}, T_{\text{ion}}) = (10^4 \text{K}, 10^4 \text{K})$  illustrates the suppression of both the amplitude of the auto-correlation and skewness functions in the presence of radiative feedback. The redshift where the minimum values of auto-correlation and skewness are reached is raised by the inclusion of feedback (given a common redshift for the completion of reionisation). The signature of radiative feedback is seen in the evolution of auto-correlation and skewness amplitude with neutral fraction. While there is substantial difference in the predicted amplitudes at neutral fractions below 0.5, the two cases are very similar before reionisation reaches a significant level. Thus the signature of radiative feedback is to suppress the amplitude of fluctuations only late in the reionisation epoch.

In a model where the minimum mass for galaxy for-

mation is  $10^5 \text{K}$  in all regions ( $T_{\min} = T_{\text{ion}} = 10^5 \text{K}$ ), the amplitudes of both the auto-correlation and skewness are substantially increased (relative to the fiducial model) at all redshifts following the onset of reionisation. Similarly, a model with  $T_{\min} = 250 \text{K}$  and  $T_{\text{ion}} = 10^5 \text{K}$  predicts amplitudes of both the auto-correlation and skewness that are substantially smaller than the fiducial model. Indeed the variation in amplitude of the auto-correlation at fixed redshift reaches an order of magnitude over the astrophysically plausible range of minimum masses. This prediction of the variation of fluctuation amplitude with the mass of ionising sources is consistent with the numerical simulations of Lidz et al. (2006). The variation is due to the larger (smaller) bias of the ionising sources, which leads to a larger (smaller) variation in ionisation state between over-dense and under-dense regions. This larger (smaller) variation in turn leads to a larger (smaller) amplitudes for both the auto-correlation and skewness functions.

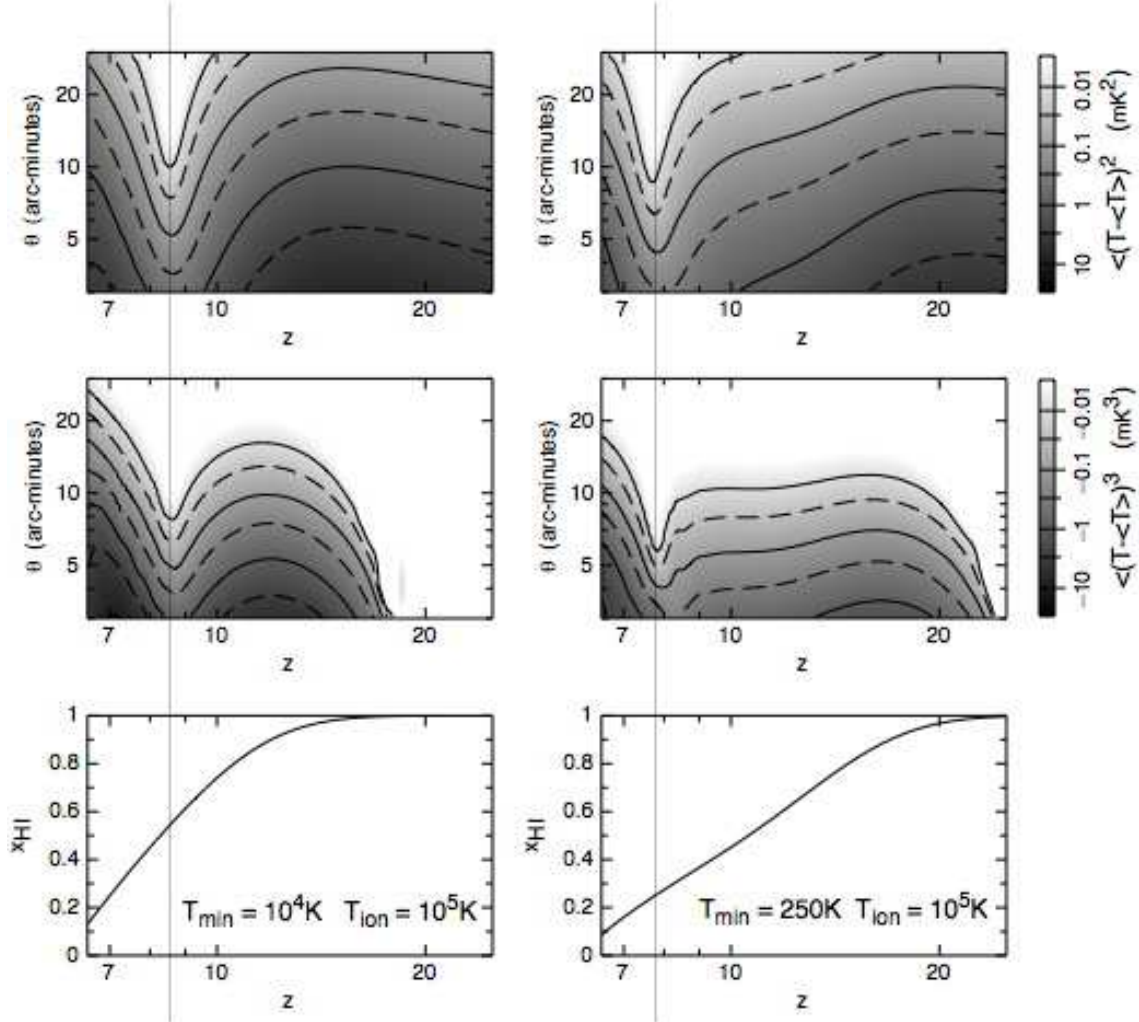


**Figure 6.** Contour plots showing the evolution of auto-correlation (upper panels) and skewness (central panels) functions with redshift and angle, assuming a clumping factor of  $C = 10$ . Two models for the minimum mass of galaxy formation are shown,  $(T_{\min}, T_{\text{ion}}) = (10^4 \text{K}, 10^5 \text{K})$  [left panels] and  $(T_{\min}, T_{\text{ion}}) = (250 \text{K}, 10^5 \text{K})$  [right panels]. The keys to the right of the panels show the numerical values assigned to the various contours. The lower panels show the evolution of average neutral fraction for these models.

All models in Figure 5 show minima of the variance and skewness at redshifts of  $z \sim 8-9$ . The duration and depth of these minima are sensitive to the bias of the ionising sources. In particular, the ratio of the auto-correlation amplitude at high redshift to the auto-correlation amplitude at the minimum varies between a factor of 10 and a factor of 100 across the models considered. Similar results are found for the skewness. The redshift of the minimum is also sensitive to the bias of the ionising sources, though the dependence is not monotonic. On the other hand there is a monotonic relation between the neutral fraction at the redshift of the minimum and the bias, with more massive ionising sources generating a minimum at a smaller ionised fraction. Models with low clumping and models with large source mass both increase the amplitude of the auto-correlation and skewness. This degeneracy between models may be broken by looking at the location of the minima in variance and skewness as functions of redshift and neutral fraction. Assuming a fixed epoch of reionisation, both large clumping factors and massive ionising sources delay the minima in time. Conversely,

a large clumping factor results in the minima occurring at a smaller average neutral fraction, while massive ionising sources lead to the minima occurring at a higher neutral fraction. However in practice the neutral fraction will be very hard to measure due to instrumental and foreground effects, which may limit the utility of this effect.

In summary the evolution of the variance and skewness in 21cm intensity maps with redshift and mean neutral fraction will probe physical quantities like the clumping of the IGM and the mass of ionising sources. In particular, reionisation scenarios with smaller values of clumping factor, or more massive (and therefore more biased) ionising sources result in 21cm intensity maps with larger values of variance and skewness. Indeed, the variation in amplitude of the auto-correlation at fixed redshift reaches an order of magnitude over the astrophysically plausible range of minimum masses. In addition, the relative locations of minima in variance and skewness when plotted as functions of redshift and neutral fraction can be used to distinguish between amplitudes that are increased due to large values of ionising

source mass, or small values of clumping factor. While more massive sources increase the amplitude of fluctuations at all epochs, the signature of radiative feedback is the suppression of fluctuations at epochs following, but not prior to the substantial reionisation of the IGM. We therefore conclude that the detection of fluctuations in 21cm intensity should unambiguously determine the mass of ionising sources.

#### 4 MEASUREMENT OF SKEWNESS IN 21CM MAPS

In the previous sections we have demonstrated that galaxy bias should lead to skewness in the intensity distribution derived from redshifted 21cm maps of the reionisation epoch. In this section we discuss the prospects for measuring that skewness using first generation instruments.

We first discuss the response of a phased array to the brightness temperature contrast of the IGM. Assuming that calibration can be performed ideally, and that foreground subtraction is perfect, the root-mean-square fluctuations in brightness temperature are given by the radiometer equation

$$\Delta T = \frac{\epsilon \lambda^2 T_{\text{sys}}}{A_{\text{tot}} \Omega_b \sqrt{t_{\text{int}} \Delta \nu}}, \quad (8)$$

where  $\lambda$  is the wavelength,  $T_{\text{sys}}$  is the system temperature,  $A_{\text{tot}}$  the collecting area,  $\Omega_b$  the effective solid angle of the synthesised beam in radians,  $t_{\text{int}}$  is the integration time,  $\Delta \nu$  is the size of the frequency bin, and  $\epsilon$  is a constant that describes the overall efficiency of the telescope. We optimistically adopt  $\epsilon = 1$  in this paper.

As a concrete example we consider the case of the Mileura Wide Field Array–Low Frequency Demonstrator (hereafter LFD<sup>1</sup>), though the measurement described could also be made using other instruments such as LOFAR<sup>2</sup>. In units relevant for the LFD, and at  $\nu = 200\text{MHz}$ , we find (Wyithe, Loeb & Barnes 2005)

$$\Delta T = 7.5 \left( \frac{T_{\text{sys}}}{250\text{K}} \right) \text{mK} \left( \frac{1.97}{C_{\text{beam}}} \right) \left( \frac{A_{\text{tot}}}{A_{\text{LFD}}} \right)^{-1} \times \left( \frac{\Delta \nu}{1\text{MHz}} \right)^{-1/2} \left( \frac{t_{\text{int}}}{100\text{hr}} \right)^{-1/2} \left( \frac{\theta_{\text{beam}}}{5'} \right)^{-2}. \quad (9)$$

Here  $A_{\text{LFD}}$  is the collecting area of a phased array consisting of 500 tiles each with 16 cross-dipoles [the effective collecting area of an LFD tile with  $4 \times 4$  cross-dipole array with 1.07m spacing is  $\sim 17 - 19\text{m}^2$  between 100 and 200MHz (B. Correy, private communication; Bowman, Morales & Hewitt 2005)]. The system temperature will be dominated by the sky and in the frequency range of interest has a value  $T_{\text{sys}} \sim 280[(1+z)/7.5]^{2.3}\text{K}$ .  $\Delta \nu$  is the frequency range over which the signal is smoothed and  $\theta_{\text{beam}}$  is the size of the synthesised beam. The value of  $\theta_{\text{beam}}$  can be regarded as the radius of a hypothetical top-hat beam, or as the variance of a hypothetical Gaussian beam. The corresponding values of the constant  $C_{\text{beam}}$  are 1 and 1.97 respectively.

Equation (9) gives the uncertainty  $\Delta T$  in the 21cm signal measured from a cylinder of IGM, with radius  $\theta$

<sup>1</sup> see <http://www.haystack.mit.edu/ast/arrays/mwa/index.html>  
<sup>2</sup> <http://www.lofar.org/>

and depth  $\Delta \nu$ . For comparison with our calculated auto-correlation and skewness, we modify this in order to estimate the noise in the signal originating from a spherical region of radius  $R$ , so that  $\theta = R/d_A$  and  $\Delta \nu/\nu = 2R(cdt/dz)^{-1}(1+z)^{-1}$  where  $\nu$  is the redshifted 21cm frequency. We find that consideration of spherical regions increases the noise relative to equation (9) by a factor of  $\sqrt{15}/8$ .

In any one synthesised beam, the measurement noise will be far in excess of the 21cm signal. However as has been discussed previously (Bowman, Morales & Hewitt 2005), the determination of the power-spectrum may still be made since it can be constructed from a large number of independent measurements (each of signal-to-noise below unity). In practice one could determine the auto-correlation function (or power-spectrum) by dividing the data stream in half, and performing a cross-correlation (Max Tegmark, private communication). Hence defining  $T$  as the measurement signal, and  $\Delta T$  as the thermal noise, we have

$$\begin{aligned} & \langle [(T - \langle T \rangle) + \Delta T_1][(T - \langle T \rangle) + \Delta T_1] \rangle \\ &= \langle (T - \langle T \rangle)^2 \rangle \\ &+ \langle (T - \langle T \rangle) \Delta T_1 \rangle + \langle (T - \langle T \rangle) \Delta T_2 \rangle + \langle \Delta T_1 \Delta T_2 \rangle, \end{aligned} \quad (10)$$

where  $\Delta T_1$  and  $\Delta T_2$  are drawn from Gaussian uncertainty distributions of width  $\sqrt{2}\Delta T$ . Here, with the exception of the first term (which is the variance), the cross-correlation results in terms that average to zero in the limit of large numbers of measurements. In a finite experiment, the sum of these terms is the measurement noise.

To estimate the noise in the measurement, we have made many Monte-Carlo realisations of the observed distribution. For each measurement we obtain  $N$  values of observed brightness temperature by adding telescope noise to the intrinsic  $T$  drawn at random from the theoretical distribution. The error for each measurement can then be calculated from the noise terms in the cross-correlation, and the uncertainty in the measurement estimated as the variance among the values of error. For a field of angular size  $\theta_{\text{field}}$  and a Gaussian synthesised beam of radius  $\theta$ , the number of independent pointings is approximated by  $N = [\theta_{\text{field}}/(2\theta)]^2$ , where the 2 in the denominator reduces the effect of overlapping synthesised beams. We assume  $\theta_{\text{field}} = 10^\circ$  for the LFD.

Comparisons of signal and noise are plotted in the upper panels of Figure 7. In both the left and right panels, the auto-correlation is plotted as a function of angle assuming  $C = 10$ , and at  $z = 6.5$ ,  $z = 8$  and  $z = 10.0$  (thin lines). For comparison we plot the estimate of noise (thick lines), assuming integrations of 100 hours (left panel) and 1000 hours (right panel). We find that the auto-correlation function can be detected at redshifts below the minimum in 100hr. In 1000 hours, higher redshift fluctuations can also be measured.

Our signal to noise estimate is approximate, and does not account for several important issues. For example, the LFD will have a very compact antenna arrangement. As a result the noise is not independent in all synthesised beams. This is because short baselines only give independent information on length scales associated with their separation. Therefore with a compact arrangement, it is only at very large scales that the pixels become independent. Moreover,

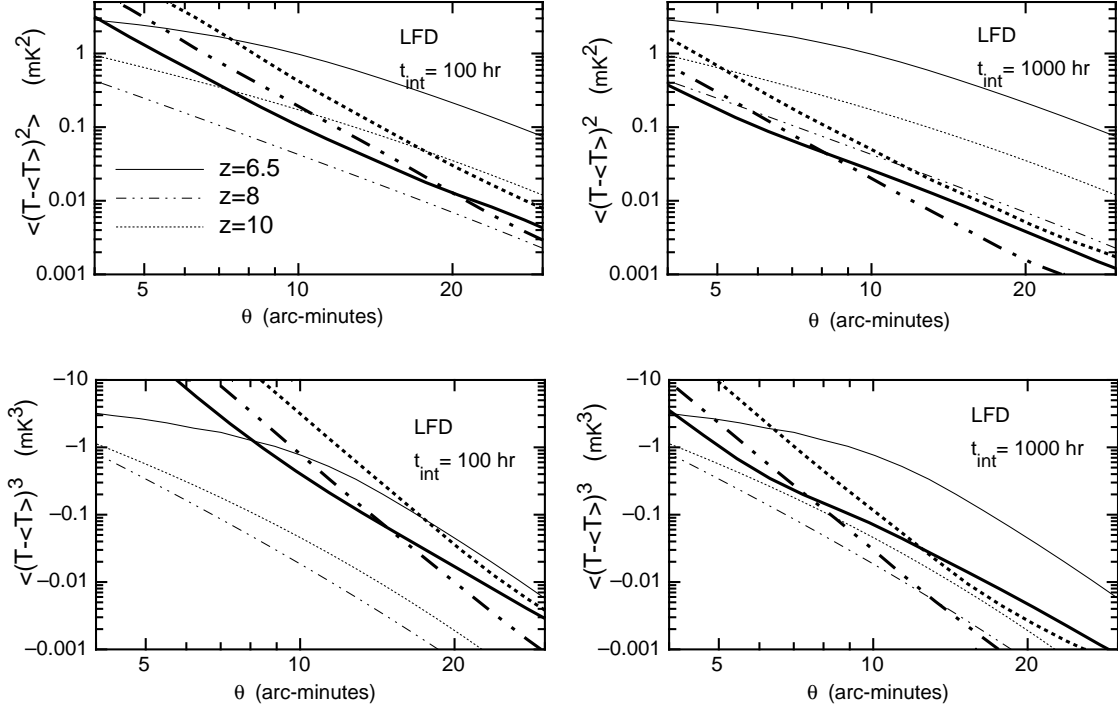


**Figure 7.** *Upper panels:* Comparisons of signal and noise for the auto-correlation as a function of angle assuming  $C = 10$ , and at  $z = 6.5$ ,  $z = 8$  and  $z = 10.0$ . The thin and thick lines correspond to signal and noise respectively. *Lower panels:* The corresponding comparisons for skewness. In each case the *left* and *right* hand panels correspond to integration times of 100 hours and 1000 hours respectively.

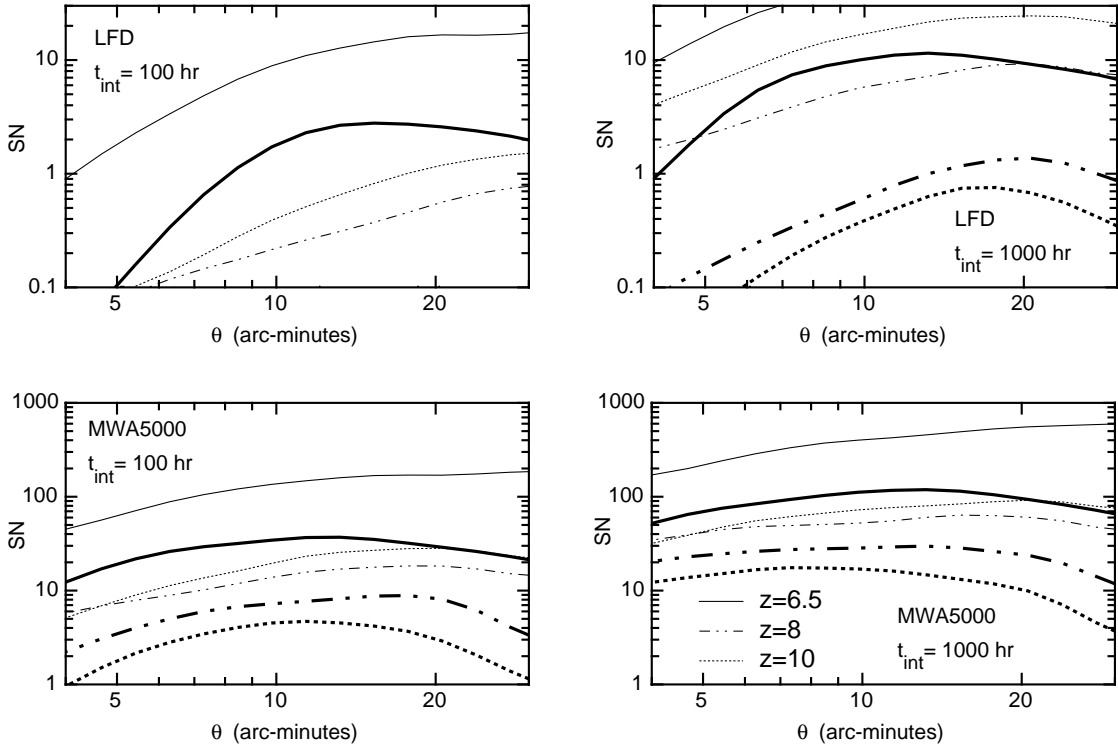


**Figure 8.** The signal-to-noise ratios for the auto-correlation (thin lines) and skewness (thick lines) functions. In each case the *left* and *right* hand panels correspond to integration times of 100 hours and 1000 hours respectively. The *upper* and *lower* rows show results for the LFD and MWA5000 respectively.

we have only considered a single frequency slice, whereas fluctuations can be measured in many slices at slightly different redshifts. This latter effect will tend to increase the sensitivity achievable relative to our estimate, while the former will tend to reduce it.

In analogy with the above procedure one could determine the skewness function by dividing the data stream in three, and performing a cross-correlation. Hence

$$\begin{aligned} & \langle [(T - \langle T \rangle) + \Delta T_1][(T - \langle T \rangle) + \Delta T_2][(T - \langle T \rangle) + \Delta T_3] \rangle \\ &= \langle (T - \langle T \rangle)^3 \rangle \\ &+ \langle (T - \langle T \rangle)^2 \Delta T_1 \rangle + \langle (T - \langle T \rangle)^2 \Delta T_2 \rangle + \langle (T - \langle T \rangle)^2 \Delta T_3 \rangle \\ &+ \langle (T - \langle T \rangle) \Delta T_1 \Delta T_2 \rangle + \langle (T - \langle T \rangle) \Delta T_1 \Delta T_3 \rangle \\ &+ \langle (T - \langle T \rangle) \Delta T_2 \Delta T_3 \rangle + \langle \Delta T_1 \Delta T_2 \Delta T_3 \rangle, \end{aligned} \quad (11)$$

where  $\Delta T_1$ ,  $\Delta T_2$  and  $\Delta T_3$  are drawn from Gaussian uncertainty distributions of width  $\sqrt{3}\Delta T$ . As before, with the exception of the first term (which is the skewness), the cross-correlation results in terms that average to zero in the limit of large numbers of measurements. In analogy with the above, we have made many Monte-Carlo measurements of the error from the noise terms in the cross-correlation, and estimated the uncertainty in the measurement of skewness from the variance among these Monte-Carlo errors.

Comparisons of signal and noise for the skewness are plotted in the lower panels of Figure 7. In both the left and right panels, the skewness is plotted as a function of angle assuming  $C = 10$ , and at  $z = 6.5$ ,  $z = 7.0$ ,  $z = 8$  and  $z = 10.0$  (thin lines). These curves correspond to the auto-correlation curves described above. For comparison we again plot the estimate of noise (thick lines), assuming integrations of 100 hours (left panel) and 1000 hours (right panel). In 100 hours, the skewness could only be (marginally) detected at lower redshifts, and at angles near  $\theta \sim 12'$ . However in 1000 hours, the skewness can be detected over a range of angles at redshifts below the minimum.

Estimates of the signal-to-noise ( $SN$ ) for measurements of the auto-correlation and skewness were obtained by taking the ratio of the signal to the root-mean-square of the sum of the noise terms in equations (10-11). The upper panels of Figure 8 show estimates of  $SN$  as a function of  $\theta$  for integrations of 100 hours and 1000 hours using the LFD. The thin lines show  $SN$  for the auto correlation function, while the thick lines show results for the skewness. In 1000 hours and at low redshift, the skewness can be detected by the LFD at a signal-to-noise as large as  $SN \sim 10$ . The  $SN$  for detection of skewness is a factor of several to 10 below that achievable for the auto-correlation function.

The above results suggest that the skewness in redshifted 21cm maps should be just detectable with the LFD. However a hypothetical follow up to the LFD would comprise  $\sim 10$  times the collecting area, with baselines of  $\sim 10$ s to 100s of kilometers (we refer to this as the MWA-5000). The signal-to-noise achievable with the MWA-5000 is plotted as a function of  $\theta$  for integrations of 100 hours and 1000 hours. In 100 hours, an MWA-5000 could detect skewness at high signal to noise outside the minimum redshift. In 1000 hours an MWA-5000 could detect skewness at all redshifts, and map out its evolution in detail. Detection of skewness would therefore be an important scientific driver for a second generation array.

## 5 CONCLUSION

Using a simple semi-analytic model for density dependent reionisation, we have quantified the extent to which galaxy bias induces skewness in the intensity distributions of redshifted 21cm maps. Our model demonstrates that skewness of the distribution is present on all scales, and during the entire reionisation era. In particular, skewness is present on scales where no single region is fully reionised. These results are consistent with the detailed numerical modeling previously presented by Lidz et al. (2006). The skewness (like the variance) decreases with increasing angular scale, but is not monotonic with redshift or neutral fraction, even in a simple reionisation scenario. A feature of our density dependent reionisation model is that it predicts a minimum in both the variance and skewness at the time when the ionisation fraction is of order 50%. This minimum is a generic feature of models that include galaxy bias, and is due to the transition between the high redshift era when the 21cm fluctuations are generated by the density field, and the lower redshift era when fluctuations are dominated by biased reionisation of the IGM.

The large scale skewness described in this paper is related to, but is different from the excess power (or bump) induced in the power-spectrum at small scales following the appearance of bubbles (Furlanetto et al. 2004). We are unable to describe the statistics of small scale fluctuations which require full numerical modeling (see e.g. Lidz et al. 2006). Skewness appears in regions of low to moderate average ionisation, and is a result of galaxy bias arising from galaxy formation within large scale over-densities. We note that if the ionisation fraction was independent of density, or even if it was a linear function of over-density, then there would be no skewness. Indeed the relation between ionisation fraction and density would be linear in the absence of galaxy bias (and of recombinations). However galaxy bias ensures a non-linear relation, and as a result, skewness of the 21cm intensity maps will be present throughout reionisation, and on all scales.

We have discussed the evolution of the amplitudes of the auto-correlation and skewness of 21cm intensity maps, as well as their evolution with redshift and mean IGM neutral fraction. The evolution of the variance and skewness in 21cm intensity maps will probe quantities like the clumping of the IGM, the mass of ionising sources and the presence of radiative feedback. For example, we find that reionisation scenarios with smaller values of clumping factor, or more massive (and therefore more biased) ionising sources result in 21cm intensity maps with larger values of variance and skewness. Indeed the variation in amplitude of the auto-correlation at fixed redshift reaches an order of magnitude over the astrophysically plausible range of minimum masses. Moreover, the relative locations of minima in variance and skewness when plotted as functions of redshift and neutral fraction can distinguish between amplitudes that are increased due to large values of ionising source mass, or small values of clumping factor. In addition, while more massive sources increase the amplitude of fluctuations at all epochs, the signature of radiative feedback is the suppression of fluctuations at epochs following, but not prior to the substantial reionisation of the IGM. We therefore conclude that the detection

of fluctuations in 21cm intensity should therefore unambiguously determine the mass of ionising sources.

We have estimated the sensitivity of the Mileura Wide-field Array Low-Frequency Demonstrator to skewness in 21cm intensity maps, and find that the predicted level should be detectable in long integrations ( $\sim 1000$  hours) at redshifts nearing the end of reionisation. However an instrument with 10 times the collecting area of the LFD could detect skewness across a range of redshifts. Skewness in 21cm maps, and a minimum in the variance during the reionisation era are generic predictions of models of reionisation that account for biased galaxy formation. The presence of this minimum in variance, and of skewness, which will be detectable at a signal-to-noise a few to ten times smaller than the variance will provide confirmation of the cosmological nature of any observed angular fluctuations.

**Acknowledgments** The research was supported by the Australian Research Council (JSBW), and by National Science Foundation grant #0457585 (MFM).

## REFERENCES

Barkana, R., & Loeb, A. 2005, ApJL, 624, L65  
 Bharadwaj, S., & Ali, S. S. 2005, MNRAS, 356, 1519  
 Bond, J. R., Cole, S., Efstathiou, G., & Kaiser, N. 1991, ApJ, 379, 440  
 Bowman, J., Morales, M., Hewitt, J., 2005, ApJ, 638, 20  
 Dekel, A., & Woo, J. 2003, MNRAS, 344, 1131  
 Dijkstra, M., Haiman, Z., Rees, M. J., & Weinberg, D. H., *Astrophys. J.*, 601, 666-675 (2004)  
 Efstathiou, G., *Mon. Not. R. Astron. Soc.*, 256, 43-47 (1992)  
 Fan, X., et al. 2006, AJ, 132, 117  
 Furlanetto, S. R., Zaldarriaga, M., & Hernquist, L. 2004, ApJ, 613, 16  
 Lidz, A., Zahn, O., McQuinn, M., Zaldarriaga, M., Dutta, S., Hernquist, L., 2006, astro-ph/0610054  
 Mo, H. J., & White, S. D. M. 1996, MNRAS, 282, 347  
 Morales, M. F., & Hewitt, J. 2004, ApJ, 615, 7  
 Press, W., Schechter, P., 1974, ApJ, 187, 425  
 Quinn, T., Katz, N., & Efstathiou, G., 278, L49-L54 (1996)  
 Spergel et al., 2006, astro-ph/0603449  
 Thoul, A. A., & Weinberg, D. H., *Astrophys. J.*, 465, 608-116 (1996)  
 White, R., Becker, R., Fan, X., Strauss, M., 2003, Astron J., 126, 1  
 Wyithe, J. S. B., Loeb, A., Barnes, D.G., 2005, ApJ, 634, 715  
 Wyithe, J. S. B., & Loeb, A. 2007, MNRAS, 375, 1034  
 Zaldarriaga, M., Furlanetto, S. R., & Hernquist, L. 2004, ApJ, 608, 622